Tant, J.; Geth, F.; Six, D.; Tant, P.; Driesen, J.; , "Multiobjective Battery Storage to Improve PV Integration in Residential Distribution Grids," Sustainable Energy, IEEE Transactions on , vol.4, no.1, pp.182-191, Jan. 2013

doi: 10.1109/TSTE.2012.2211387

URL:
http://ieeexplore.ieee.org/stamp/stamp.jsp?tp=&arnumber=6305498&isnumber=6380594

Multi-Objective Battery Storage to Improve PV Integration in Residential Distribution Grids

Jeroen Tant, *Graduate Student Member, IEEE,* Frederik Geth, *Graduate Student Member, IEEE,* Daan Six, Peter Tant, and Johan Driesen, *Senior Member, IEEE*

***Abstract*—This paper investigates the potential of using battery energy storage systems in the public low-voltage distribution grid, to defer upgrades needed to increase the penetration of PV. A multi-objective optimization method is proposed to visualize the trade-offs between three objective functions: voltage regulation, peak power reduction and annual cost. The method is applied to a near-future scenario, based on a real residential feeder. The results provide insight into the dimensioning and the required specifications of the battery and the inverter. It is found that an inverter without batteries already achieves part of the objectives. Therefore, the added value of batteries to an inverter is discussed. Furthermore, a comparison between lithium-ion and lead-acid battery technologies is presented.**

***Index Terms*—Battery energy storage system, residential distribution grid, multi-objective optimization, peak shaving, photovoltaics, voltage regulation**

NOMENCLATURE

S_{nom}	Nominal inverter apparent power (kVA).
E_{nom}	Nominal battery capacity (kWh).
E_{eff}	Effective battery capacity (kWh).
$P_{\text{nom}}^{\text{dc}}$	Nominal dc-link power (kW).
$P_{p,k}^{\text{inv}}$	Inverter three-phase active power profile (kW).
$Q_{p,k}^{\text{inv}}$	Inverter three-phase reactive power profile (kvar).
$\Delta U_{\text{rms}}^{\text{peak}}$	Objective function for voltage regulation (V).
$S_{\text{rms}}^{\text{peak}}$	Objective function for peak shaving (kVA).
$U_{p,h,k}$	Complex line-to-neutral voltage in house h (V).
$P_{p,k}^{\text{tot}}$	Grid total active power consumption (kW).
$\lvert S_{p,k}^{\text{tot}} \rvert$	Grid total apparent power consumption (kVA).
K_{tot}	Total cost (€/a).
K_{E}	Energy cost (€/a).
m_k	Electricity tariff profile (€/kWh).
$\tau_{\text{E}}^{\text{bat}}$	Battery calendar life (a).
n_{cycles}	Number of battery cycles (a^{-1}).

Manuscript received February 7, 2012; revised April 28, 2012; accepted July 13, 2012.

The work is supported by the Flemish Government through the LINEAR project (IWT/090800) organized by the Institute for Science and Technology (IWT). J. Tant has a Ph.D. fellowship of the Research Foundation - Flanders (FWO).

J. Tant, F. Geth, P. Tant, and J. Driesen are with the Research Group ELECTA, Department of Electrical Engineering, KU Leuven, Leuven 3000, Belgium (e-mail: jeroen.tant@esat.kuleuven.be; frederik.geth@esat .kuleuven.be; johan.driesen@esat.kuleuven.be).

D. Six is with VITO, the Flemish Institute for Technological Research, Mol 2400, Belgium (e-mail: daan.six@vito.be).

KU Leuven and VITO are partners of Energyville, Genk 3600, Belgium

Digital Object Identifier: xxxxxxxxxxx

I. INTRODUCTION

THE potential of battery energy storage systems (BESS) to support the operation of public distribution grids gains wide interest [1], [2]. This paper focuses on the application of BESS in a low voltage (LV) distribution feeder with local photovoltaics (PV), applied to the Flanders region in Belgium and in the framework of the LINEAR research on active demand [3].

It is known that residential PV systems connected to an existing LV feeder cause overvoltage problems in some situations [4]–[9]. Currently, country-specific regulations require PV inverters to disconnect automatically when a maximum voltage limit is exceeded [9]–[11]. These type of disconnections occur presently in practice in Belgium, because of the recent growth in the number of residential PV installations [9]. Therefore, in some feeders, the overvoltage problem puts a limit on the amount of PV that can be installed without further grid reinforcements [9]. Expensive grid upgrades could be postponed or prevented by regulating voltage peaks locally.

One method to reduce voltage rise is the curtailment of active power injected into the grid. To avoid losses, PV owners can store the curtailed energy in batteries indoors [5]. An implicit option to curtail injected power is a feed-in tariff that favors self-consumption, which gives an incentive to install batteries [8], [12]. In some countries, such an incentive system already exists, for instance in Germany [6].

A second method to accomplish voltage regulation is the injection of reactive power into the grid by using the PV inverters already present [7], [8]. In Germany, new PV inverters are already required to have the capability to provide a static amount of reactive power [9]. However, the amount of reactive power that can be injected appears to be limited by components in the MV and LV distribution grid, such as the LV transformer [8].

This paper considers the possibility of connecting a BESS locally, in problematic distribution grids [13]. A BESS could mitigate both overvoltage and overload problems at the same time, by combining voltage regulation and peak shaving strategies. Voltage regulation with active and reactive power could defer grid upgrades and allow a higher amount of installed PV. The peak shaving application could defer investments needed to upgrade overloaded components [2], by minimizing peak apparent power locally. A combination of multiple services with a single BESS has been suggested in [8]. However, a method should be found to deal with the trade-off between the quality of the delivered services [14]. Therefore, for a

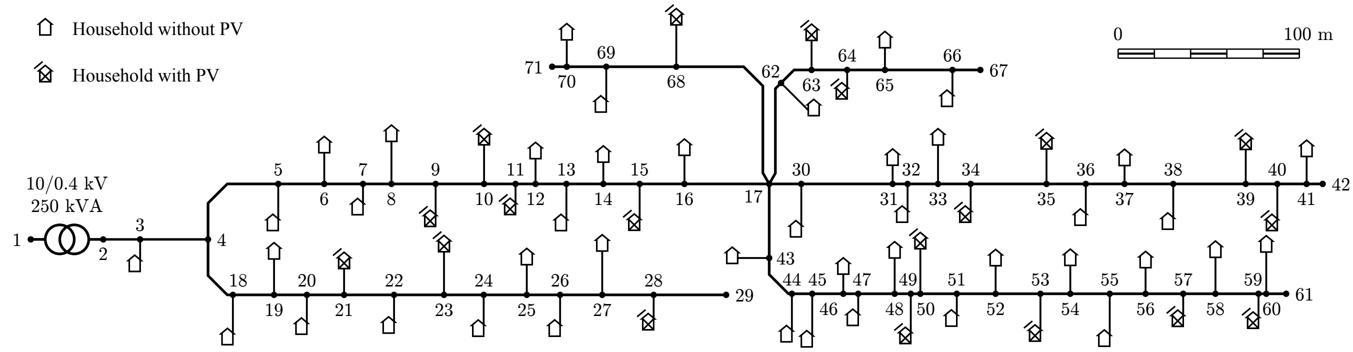

Fig. 1. Schematic diagram of the semi-urban feeder used in the scenario. Cable lengths are drawn to scale.

feasibility assessment of BESS, a multi-objective optimization method is appropriate.

The optimization model presented in this paper is a continuation of previous work [14], [15]. In [14], a multi-objective genetic algorithm was used to determine the location, size and optimal power flow of multiple BESS units in a 24 kV MV grid. A simple BESS model was used to demonstrate the possible trade-offs between benefits for stakeholders. In [15], the BESS model was extended to include an estimation of life expectancy, in order to determine investment cost and depreciation cost. This model was used to determine the trade-off control strategy for cost optimization and peak shaving for one single-phase household with PV. In this paper, the BESS model is further extended to include a three-phase inverter with bidirectional active and reactive power flow. A three-phase unbalanced grid model is included to determine grid voltages.

A continuous multi-objective optimization technique is proposed, which allows for clear visualization of trade-off curves between annual cost and the performance of voltage control and peak shaving. Both the BESS design variables and BESS power flow time profiles are optimized together.

The optimization method is applied to a reference scenario of a LV distribution feeder. The influence of the location of the BESS in the feeder is analyzed. Secondly, the added value of batteries to an inverter is discussed. It will be shown that, to a certain amount, voltage control and peak shaving is also possible with an inverter without batteries through power exchange between the phases of the unbalanced grid. Furthermore, the rigorous optimization approach allows for a fair comparison between lithium-ion and lead-acid battery technologies.

II. Reference Scenario Description

A. Grid Topology

The proposed scenario uses a $230/400$ V reference grid, based on the topology of a real semi-urban feeder with a TT earthing arrangement in the region of Flanders, Belgium [3]. A schematic diagram of this three-phase distribution feeder with underground four-wire cables is shown in Fig. 1.

Cable parameters are listed in Table I. The impedance values are calculated according to design specifications in the Belgian standard for underground distribution cables NBN C33-322 [16] with an assumed operating temperature of $45\ ^\circ\mathrm{C}$. The grid frequency is 50 Hz. All main feeder cables are of type EAXVB 1 kV $4 \times 150\ \mathrm{mm}^2$ except for the cable between nodes 2 and 4, which is of type EAXVB 1 kV $4 \times 95\ \mathrm{mm}^2$. A 250 kVA $10/0.4$ kV transformer is assumed with an impedance of $0.013 + 0.038\mathrm{j}$ pu.

TABLE I
CABLE PARAMETERS

Cable Type	Impedance at $45\ ^\circ\mathrm{C}$
EAXVB 1 kV $4 \times 95\ \mathrm{mm}^2$	$0.352 + 0.078\mathrm{j}\ \Omega/\mathrm{km}$
EAXVB 1 kV $4 \times 150\ \mathrm{mm}^2$	$0.227 + 0.078\mathrm{j}\ \Omega/\mathrm{km}$
EXVB 1 kV $4 \times 16\ \mathrm{mm}^2$	$1.265 + 0.083\mathrm{j}\ \Omega/\mathrm{km}$

Cables running from the supply terminal of each house to the main feeder are of type EXVB 1 kV $4 \times 16\ \mathrm{mm}^2$, with a randomly assigned length between 10 m and 25 m. In this scenario, all 62 houses are assumed to have a single-phase connection between one phase and the neutral conductor, with a nominal line-to-neutral voltage U_{nom} of 230 V. The houses have an alternating phase assignment as shown in the first column of Fig. 2.

B. Household Load Profiles

A set of 62 household electricity consumption profiles was measured in 2007 by two DSOs, at households that are statistically representative for Flanders [3]. Reactive power consumption was not measured and is therefore neglected.

A single-phase PV generation profile is assigned to 19 of 62 houses, corresponding to a PV penetration level of 30.6 %. Because of the correlation between PV generation profiles of nearby houses, only one single PV profile is used. This profile is rescaled for each house to cover 100 % of the household annual energy consumption, while considering commercially available inverter sizes and the maximum single-phase grid injection limit of 5 kW imposed by regulations [10]. The profile was measured in 2008 at a fixed rooftop PV installation at KU Leuven, and realigned in time to match with the consumption profiles of 2007.

Out of the year 2007, 16 full weeks are selected randomly and all profiles are reduced to this 16-week length. The time step T_{s} of the time profiles is 15 minutes, resulting in a number of time steps n_t equal to 10752. For each house, the household

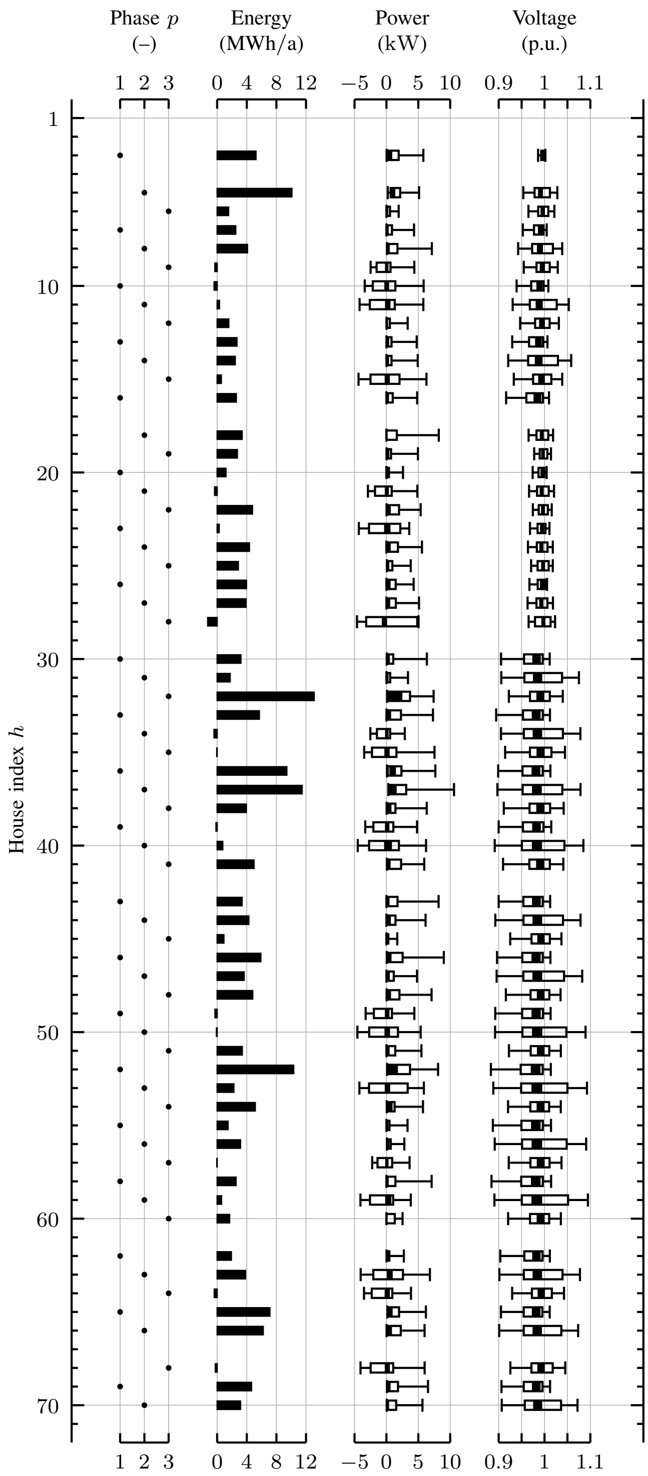

Fig. 2. Household scenario: phase assignment for each house (column 1), statistical properties of the household net power profiles (columns 2 and 3) and the distribution of voltage profiles inside every home (column 4).

profile and PV generation profile are combined into one net power profile. The distribution of the net power profiles is displayed in the third column of Fig. 2. The corresponding annual energy consumption is displayed in column two. In this figure, and throughout the rest of this paper, a modified box plot is used to display the distribution of time profiles. Its structure is defined in Fig. 3. An additional box, spanning the

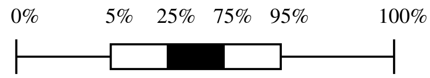

Fig. 3. Modified box plot used throughout this paper to represent the distribution of time profiles. The inner box spans the 25th to 75th percentiles and the outer box spans the 5th to 95th percentiles. The whiskers extend to the minimum and maximum values.

5th to 95th percentiles, is added to the standard box plot in order to emphasize peak values, which are of interest in this paper.

C. Load Flow Analysis

A load flow method for three-phase unbalanced radial grids is implemented in MATLAB, based on the backward–forward sweep technique [17]. The voltages at the supply terminal of every house are calculated at each time step, for the described scenario without BESS. A constant power load model is assumed. The fourth column of Fig. 2 shows the statistical distribution of calculated voltages. All voltages are within the $U_{\text{nom}} \pm 5\ \%$ range for $90\ \%$ of the time. At some locations, the voltage peak value approaches the $U_{\text{nom}} + 10\ \%$ limit in phase 2 and exceeds the $U_{\text{nom}} - 10\ \%$ limit in phases 1 and 2.

The European standard EN50160 states that the 10-minute mean rms voltage deviation should not exceed $\pm 10\ \%$ of the nominal voltage and in the test procedure a wider range from $-15\ \%$ to $+10\ \%$ is allowed for $5\ \%$ of the time per week [18]. The PV inverter automatic disconnection devices will disconnect from the grid when the 10-minute mean rms voltage, measured at the inverter, exceeds $110\ \%$ of the nominal voltage [10], [11]. In the load flow calculation, the voltage drop between the PV inverter and main supply terminal is not taken into account. Therefore, it is likely that some of the inverters connected to phase 2 disconnect in practice.

The load flow results are in compliance with the EN50160 standard, but there is limited margin to increase the amount of PV in this feeder. Similar results were found in [4], where the PV penetration level of $50\ \%$ had to be reduced to $30\ \%$ to be acceptable.

D. Market Scenario

A dynamic electricity tariff is imposed, based on the baseline scenario defined in [19]. The electricity price profile, m_k, is given by

$$m_k = \left(0.44 + 0.56 \cdot \overline{m}_k^{\text{BPX}}\right) \cdot 0.171\ \text{€/kWh} \tag{1}$$

where $\overline{m}_k^{\text{BPX}}$ is the normalized wholesale price at time step k on the Belpex day-ahead market for electricity of 2007. The $0.171\ \text{€/kWh}$ value corresponds to the average electricity price paid by residential consumers in Flanders in 2010 [19]. The fraction of 0.44 represents the constant distribution costs (0.35), transmission costs (0.08) and levies (0.01). The 0.56 fraction represents the variable energy costs [20].

III. BESS Model

A. Technical Model

The battery of the considered BESS is connected to the dc-bus of a grid-tied inverter, capable of providing active and reactive power in four quadrants for each phase individually. This functionality requires three single-phase inverters with a common dc-bus, or one three-phase four-wire inverter [21]. The inverter complex output power in phase p at time step k is given by

$$S_{p,k}^{\text{inv}} = P_{p,k}^{\text{inv}} + \mathrm{j}Q_{p,k}^{\text{inv}} \qquad p = 1,2,3 \tag{2}$$

and is limited by the inverter nominal apparent power, S_{nom}:

$$\left|S_{p,k}^{\text{inv}}\right| \leq \frac{S_{\text{nom}}}{3} \qquad p = 1,2,3. \tag{3}$$

The bidirectional power flow from the inverter to the battery is split into two positive complementary variables: the charge power P_k^{c} and the discharge power P_k^{d}. Only one of these variables is allowed to be nonzero at each time step k.

$$P_k^{\text{c}} P_k^{\text{d}} = 0. \tag{4}$$

Both are limited by the nominal power of the dc-link between the battery cells and the inverter, $P_{\text{nom}}^{\text{dc}}$:

$$0 \leq P_k^{\text{c}} \leq P_{\text{nom}}^{\text{dc}}, \quad 0 \leq P_k^{\text{d}} \leq P_{\text{nom}}^{\text{dc}}. \tag{5}$$

Additionally, the maximum charge and discharge power is dependent on the battery technology:

$$P_k^{\text{c}} \leq \gamma_{\text{c}} E_{\text{nom}}, \quad P_k^{\text{d}} \leq \gamma_{\text{d}} E_{\text{nom}}, \tag{6}$$

where E_{nom} is the nominal battery capacity, and γ_{c} and γ_{d} are the charge and discharge power-to-energy ratios. The balance equation for active power is given by

$$P_k^{\text{d}} - P_k^{\text{c}} = \rho_{\text{sb}} S_{\text{nom}} + \sum_{p=1}^{3} \left(P_{p,k}^{\text{inv}} + (1-\eta_{\text{inv}})\left|S_{p,k}^{\text{inv}}\right|\right), \tag{7}$$

where η_{inv} is the inverter efficiency. The nominal power specific loss ρ_{sb} represents losses from peripherals such as control, safety, and ventilation systems.

The battery energy content at time step k, E_k, satisfies the recurrence relation

$$E_k = E_{k-1} + \eta_{\text{c}} T_{\text{s}} P_k^{\text{c}} - \frac{1}{\eta_{\text{d}}} T_{\text{s}} P_k^{\text{d}}. \tag{8}$$

where T_{s} is the time step, and η_{c} and η_{d} are the charge and discharge efficiency, respectively. The initial and final energy content are defined as:

$$E_0 = \frac{1}{2} E_{\text{eff}}, \quad E_{n_t} \geq \frac{1}{2} E_{\text{eff}}, \tag{9}$$

where n_t is the number of time steps. The variable E_{eff} is the effective battery capacity and serves as an imposed limit on the battery energy content:

$$0 \leq E_k \leq E_{\text{eff}} \leq E_{\text{nom}}. \tag{10}$$

A reduction of E_{eff} extends the battery cycle life [22]. The cycle life is defined as the number of charge–discharge cycles that can be performed before the remaining usable capacity falls below 80 % of the nominal battery capacity, due to wear [22]. In this paper, the ratio of decision variables E_{eff} to E_{nom} is constrained to the interval

$$0.05 \leq \frac{E_{\text{eff}}}{E_{\text{nom}}} \leq 0.8. \tag{11}$$

The 80 % limit ensures that the effective energy capacity is available during the entire cycle life. It is assumed that the battery is replaced when the cycle life is reached. Depending on the E_{eff} to E_{nom} ratio, the battery cycle life is parameterized as [23]:

$$n_{\text{cycle-life}} = n_{80} \left(\frac{1}{0.8} \frac{E_{\text{eff}}}{E_{\text{nom}}}\right)^q, \tag{12}$$

where n_{80} is the cycle life at an E_{eff} to E_{nom} ratio of 80 %. The exponent $q \leq 0$ can be determined by fitting the proposed curve to manufacturer data. The average number of charge–discharge cycles performed by the BESS per unit of time is given by [24]:

$$n_{\text{cycles}} = \frac{\eta_{\text{c}} \sum_{k=1}^{n_t} P_k^{\text{c}}}{n_t E_{\text{eff}}}. \tag{13}$$

Next to the cycle life, the battery also has a limited shelf life $\tau_{\text{E,sl}}^{\text{bat}}$, independent of battery usage. The calendar life $\tau_{\text{E}}^{\text{bat}}$ is then defined as the minimum of cycle life and shelf life:

$$\tau_{\text{E}}^{\text{bat}} = \min\left(\frac{n_{\text{cycle-life}}}{n_{\text{cycles}}}, \tau_{\text{E,sl}}^{\text{bat}}\right). \tag{14}$$

This calendar life is assumed to correspond to the actual battery lifetime and is used in the following section to calculate the battery depreciation cost.

B. Cost Model

The total BESS cost per year, K_{tot}, is split into three components [15], [25]:

$$K_{\text{tot}} = K_{\text{depr}} + K_{\text{fix}} + K_{\text{E}}. \tag{15}$$

The first component, K_{depr}, encompasses the depreciation costs of the battery, battery peripherals, and inverter. The battery lifetime $\tau_{\text{E}}^{\text{bat}}$ is determined with (14). The battery peripherals lifetime $\tau_{\text{P}}^{\text{bat}}$ and inverter lifetime $\tau_{\text{P}}^{\text{inv}}$ are assumed to be independent of other variables in the model. The K_{depr} component is given by

$$K_{\text{depr}} = \frac{c_{\text{E}}^{\text{bat}} E_{\text{nom}}}{\tau_{\text{E}}^{\text{bat}}} + \frac{c_{\text{P}}^{\text{bat}} P_{\text{nom}}^{\text{dc}}}{\tau_{\text{P}}^{\text{bat}}} + \frac{c_{\text{S}}^{\text{inv}} S_{\text{nom}}}{\tau_{\text{P}}^{\text{inv}}}, \tag{16}$$

where $c_{\text{E}}^{\text{bat}}$, $c_{\text{P}}^{\text{bat}}$, and $c_{\text{S}}^{\text{inv}}$ are the specific investment costs of the battery, battery peripherals, and inverter respectively.

The second component encompasses the fixed capital costs and maintenance costs. These costs are assumed to be 10 % of the initial BESS investment cost [25]:

$$K_{\text{fix}} = \left(c_{\text{E}}^{\text{bat}} E_{\text{nom}} + c_{\text{P}}^{\text{bat}} P_{\text{nom}}^{\text{dc}} + c_{\text{S}}^{\text{inv}} S_{\text{nom}}\right) \cdot 10\ \%/\text{a}. \tag{17}$$

The final component is the average energy cost per unit of time, dependent on the electricity price profile and the active power flow between the inverter and the grid:

$$K_{\text{E}} = -\frac{1}{n_t} \sum_{k=1}^{n_t} m_k \left(P_{1,k}^{\text{inv}} + P_{2,k}^{\text{inv}} + P_{3,k}^{\text{inv}}\right). \tag{18}$$

TABLE II
BATTERY PARAMETERS

	Li–ion	Pb–acid	
Cycle life at $E_{\text{eff}}/E_{\text{nom}} = 80\ \%$ n_{80}	3000	400	(–)
Cycle life exponent q	-1.825	-1.607	(–)
Charge efficiency η_{c}	88.2	78.4	(%)
Discharge efficiency η_{d}	98.0	98.0	(%)
Charge power-to-energy ratio γ_{c}	1	$\frac{1}{3}$	(h^{-1})
Discharge power-to-energy ratio γ_{d}	4	1	(h^{-1})
Nominal energy specific cost $c_{\text{E}}^{\text{bat}}$	1000	250	(€/kWh)
Nominal power specific cost $c_{\text{P}}^{\text{bat}}$	270	0	(€/kW)
Battery peripherals lifetime $\tau_{\text{P}}^{\text{bat}}$	10	10	(a)
Shelf life $\tau_{\text{E,sl}}^{\text{bat}}$	10	10	(a)

TABLE III
INVERTER PARAMETERS

Inverter efficiency	η_{inv}	97	%
Nominal power specific auxiliary losses	ρ_{sb}	1	%
Nominal power specific cost	$c_{\text{S}}^{\text{inv}}$	230	€/kVA
Inverter lifetime	$\tau_{\text{P}}^{\text{inv}}$	10	a

C. Battery and Inverter Parameters

The battery parameters for the simulation scenario are listed in Table II. This set of parameters is in line with previous work [15], literature [23], [25], [26], and commercially available products. Two currently available technologies are considered: lithium iron phosphate (Li–ion) batteries and absorbed glass mat lead–acid (Pb–acid) batteries. The Coulomb efficiency is included in the charge efficiency parameter η_{c}. Therefore, the η_{c} value is less than the discharge efficiency η_{d}, which only includes the dc-link efficiency. The efficiency is modeled as independent of current and temperature.

Li–ion batteries require a management system for cell balancing and protection [27]. The cost of this system is represented by the parameter $c_{\text{P}}^{\text{bat}}$, proportional to the nominal dc-link power.

The inverter parameters are listed in Table III. The value for the specific inverter cost, $c_{\text{S}}^{\text{inv}}$, is based on [28]. The inverter efficiency was found in [6]. The expected inverter lifetime $\tau_{\text{P}}^{\text{inv}}$ and the expected battery peripherals lifetime $\tau_{\text{P}}^{\text{bat}}$ are assumed to be equal to 10 years. The inverter life expectancy can be estimated with given manufacturer data (e.g. the manufacturer warranty period) or with detailed reliability studies [29].

IV. MULTI-OBJECTIVE OPTIMIZATION

A. Objective Functions

Three objective functions are to be minimized. They are evaluated over a period of one year, statistically represented by time profiles with a length of 16 weeks.

The first objective function is a performance indicator for voltage regulation. Four houses are selected at the ends of the feeder, as feedback points where the three-phase indoor voltage is measured. These houses are grouped in the index set

$$\mathcal{H}_{\text{m}} = \{41, 60, 66, 70\}. \tag{19}$$

The relationship between BESS output power, $S_{\tilde{p},k}^{\text{inv}}$, and the modulus of the complex voltage at every house in the set $\mathcal{H}_{\text{m}}$, $|U_{p,h,k}|$, is approximated with a linear model:

$$|U_{p,h,k}| = \left|U_{p,h,k}^{0}\right| + \sum_{\tilde{p}=1}^{3} \left(c_{p,\tilde{p},h,k}^{P} P_{\tilde{p},k}^{\text{inv}} + c_{p,\tilde{p},h,k}^{Q} Q_{\tilde{p},k}^{\text{inv}} \right), \tag{20}$$

where $U_{p,h,k}^{0}$ is the exact load flow solution without BESS. The derivatives $c_{p,\tilde{p},h,k}^{P}$ and $c_{p,\tilde{p},h,k}^{Q}$ are obtained for each time step by numerical differentiation of the load flow equations. These derivatives are also dependent on the battery location.

When voltage regulation is used to defer grid upgrades, it is of interest to minimize peak values. Therefore, for every day, the maximum peak voltage deviation is determined. The proposed objective function for voltage regulation is defined as the rms value of all daily peak deviations in the evaluation period:

$$\Delta U_{\text{rms}}^{\text{peak}} = \sqrt{\frac{1}{n_d} \sum_{d=1}^{n_d} \max_{\substack{k \in \mathcal{K}_d, h \in \mathcal{H}_{\text{m}} \\ p \in \{1,2,3\}}} \left(|U_{p,h,k}| - U_{\text{nom}}\right)^2}, \tag{21}$$

where U_{nom} is the nominal grid voltage, n_d is the number of days in the evaluation period, and $\mathcal{K}_d$ is the set of time steps in day d.

Similar reasoning is applied to compose the second objective function, which is the performance indicator for peak shaving. The total complex power consumption in phase p is obtained by adding the inverter output power in phase p to the power profiles of all households connected to phase p:

$$S_{p,k}^{\text{tot}} = P_{p,k}^{\text{inv}} + \text{j}Q_{p,k}^{\text{inv}} + \sum_{h \in \mathcal{H}_p} P_{h,k}, \tag{22}$$

where $P_{h,k}$ is the load profile of house h, and $\mathcal{H}_p$ is the set of houses connected to phase p. The objective function for peak shaving is then given by the rms value of daily peak apparent power:

$$S_{\text{rms}}^{\text{peak}} = \sqrt{\frac{1}{n_d} \sum_{d=1}^{n_d} \max_{\substack{k \in \mathcal{K}_d, \\ p \in \{1,2,3\}}} \left|S_{p,k}^{\text{tot}}\right|^2}. \tag{23}$$

The third objective function is the total annual cost K_{tot} determined by (15) and enables the optimization algorithm to calculate the trade-off between performance and cost. Furthermore, through (18), the BESS can take advantage of price volatility to purchase energy at a low price, and sell back energy at higher price. However, in order to turn this extra revenue into overall profit, battery prices should decrease further [25]. Nevertheless, in combination with the other objective functions, the extra revenue is used to reduce overall costs.

B. Decision Variables

The decision variables in the multi-objective optimization model can be divided into design variables and control variables. The design variables are the inverter nominal power S_{nom}, the battery nominal capacity E_{nom}, the battery effective capacity E_{eff}, and the dc-link nominal power $P_{\text{nom}}^{\text{dc}}$. The $P_{\text{nom}}^{\text{dc}}$ variable can take a lower value than the limit defined by the battery technology in (6), in order to save costs in the design of the battery management system. A reduction of the E_{eff} to E_{nom} ratio extends battery cycle life, as shown in (12). However, a larger and more expensive battery would then be needed to provide the same effective energy capacity. Therefore, E_{eff} and E_{nom} are both chosen as decision variables to be determined by the optimization algorithm.

The control decision variables are the inverter active and reactive power set points for each time step and phase, $P_{p,k}^{\text{inv}}$ and $Q_{p,k}^{\text{inv}}$, used by the optimization algorithm to determine the Pareto-optimal control strategy of the BESS. The battery energy state E_k, charge power P_k^{c}, and discharge power P_k^{d} are dependent on $P_{p,k}^{\text{inv}}$ and $Q_{p,k}^{\text{inv}}$.

C. Optimization Problem

The multi-objective problem is reformulated as an optimization problem with one combined objective. The objective functions for voltage regulation and peak shaving are squared and linearly combined with a weight factor $0.01 \leq w \leq 0.99$. The total annual cost objective K_{tot} is constrained to a maximum allowed cost $K^{\max}$. The optimization problem is also subject to constraints defined by the model equations. The problem is formulated as:

$$\begin{aligned} \text{minimize} \quad & w \Delta {U_{\text{rms}}^{\text{peak}}}^2 + (1-w)\, {S_{\text{rms}}^{\text{peak}}}^2 \\ \text{subject to} \quad & K_{\text{tot}} \leq K^{\max} \\ & \text{(2)–(18), (20), (22).} \end{aligned} \tag{24}$$

In the results section of this paper, the trade-off curve between $\Delta U_{\text{rms}}^{\text{peak}}$ and $S_{\text{rms}}^{\text{peak}}$ for a fixed $K^{\max}$ is obtained by solving (24) for multiple weight factors w.

D. Algorithm and Approximations

In order to solve (24) efficiently, some approximations and optimization tricks are applied. A first approximation was already applied in (20) by linearizing the load flow equations. The operator for the magnitude of complex power as used in (3), (7) and (23), is modeled by introducing an auxiliary decision variable S_{aux} with a quadratic circular constraint:

$$|S| = S_{\text{aux}}, \quad S_{\text{aux}}^2 \geq P^2 + Q^2. \tag{25}$$

The constraint is modeled as an inequality, to obtain a convex constraint. Furthermore, the quadratic constraint is approximated with an eight-sided regular polygon (see the Appendix), to obtain a set of linear constraints. Because of the inequality, S_{aux} is allowed to be higher than necessary. However, this would result in a suboptimal result in the case of equation (23), and in additional power dissipation in the case of equation (7). Although this extra power dissipation is not observed in the results of this paper, it could exist, for example, in a scenario with negative energy prices. The same reasoning applies to the nonlinear constraint (4). A violation of this constraint would imply an additional power dissipation in (8). The constraint is omitted while solving the optimization problem, and checked for validity afterwards.

The time profiles P_k^{c} and P_k^{d} are modeled with auxiliary decision variables, as well as the E_k time profile, which allows the recurrence relation (8) to be modeled as a sparse system of equality constraints. The maximum value operators in (21) and (23) are also modeled by introducing auxiliary variables constrained to be higher than the operator's arguments. The minimum value operator in (14), is reformulated into a maximum value operator after division in (16).

With the discussed approximations, the objective function of (24) is quadratic and all constraints are linear, except for one constraint determining K_{depr} through equations (12), (13) and (14), which is nonlinear and nonconvex. Therefore, the problem is categorized as a nonlinear problem and is solved with sequential quadratic programming (SQP). Only one constraint has to be linearized in each SQP iteration. The quadratic subproblems are solved with the ILOG CPLEX barrier optimizer, an interior point method suited for large, sparse problems. The optimization problem is implemented in MATLAB with the modeling toolbox YALMIP [30].

V. Results

The solutions of the multi-objective optimization problem are presented as isocost trade-off curves between the objectives of peak shaving and voltage control. Each trade-off curve is a Pareto front with multiple set points for the design variables and control strategy of the BESS. The maximum cost displayed in the result figures is €5000 per year. In comparison, the total annual cost of all electricity consumed by the 62 households in the scenario feeder, without PV, is equal to €50 766, with a distribution cost component of €16 567 (see section II-D).

First, the proposed optimization method is used to determine the optimal location of the BESS in the reference grid. Then, the added value of batteries to an inverter, with respect to the objective functions, is studied. Finally, Li–ion and Pb–acid battery technologies are compared.

A. Optimal BESS Location

Fig. 4 visualizes the performance of BESS with Li–ion batteries for a maximum cost of €5000 per year at different locations. The possible BESS locations are the nodes without a connected house in Fig. 1, and correspond in practice to locations where junction boxes are available. Although the curve for node 17 dominates all other solutions, the sensitivity of the voltage regulation objective to the BESS location is low for nodes far enough from the transformer (nodes 42, 61, 67, and 71), compared to nodes close to the transformer (node 2 and 4). The peak shaving objective is not dependent on the BESS location. In the remainder of this paper, node 17 is used as the BESS location.

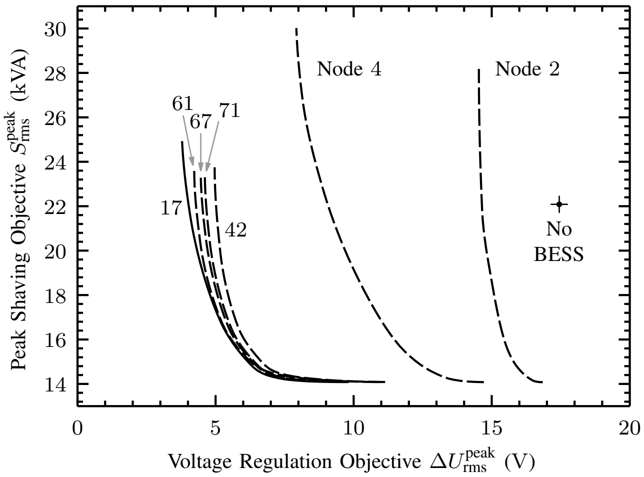

Fig. 4. Pareto-optimal trade-off curves between the objectives of peak shaving and voltage regulation, computed for different BESS locations. The total cost is fixed at €5000 per year and the battery technology is Li–ion.

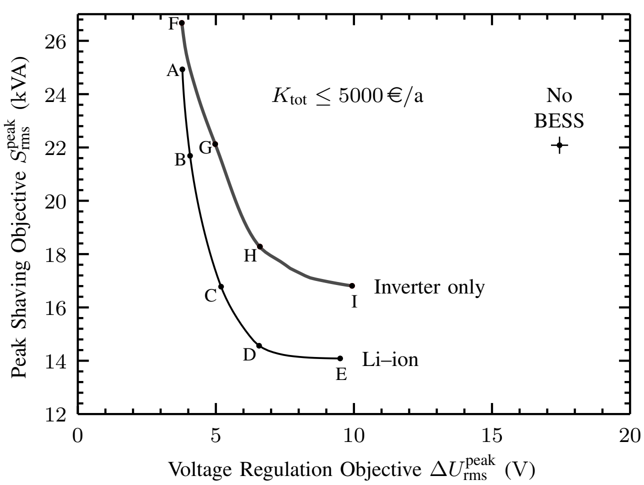

Fig. 5. Pareto-optimal trade-off curves between the objectives of peak shaving and voltage regulation, computed for a BESS with Li–ion batteries and an inverter without batteries; both connected at node 17. The maximum cost is €5000 per year.

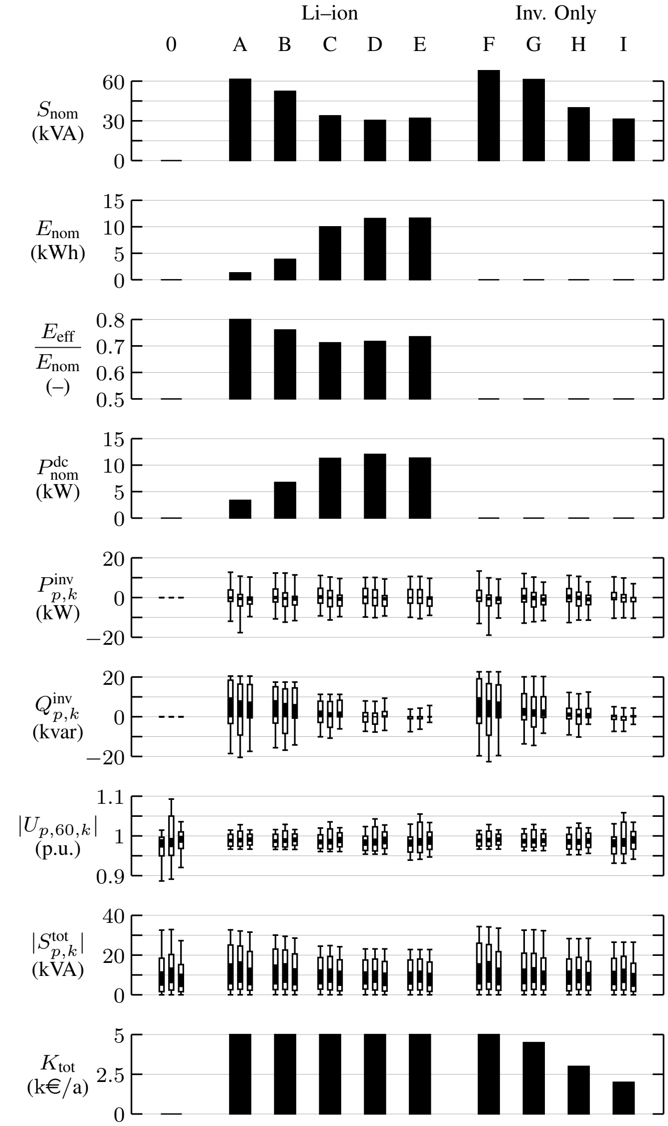

Fig. 6. Decision variables for the solutions A to I depicted in Fig. 5.

B. Added Value of Batteries

Fig. 5 shows the trade-off curves for a BESS with Li–ion batteries (A to E) and for an inverter without batteries (F to I), for a maximum cost of €5000 per year. The corresponding decision variables are represented in Fig. 6.

The Li–ion curve is considered first. Point A matches with a strategy of voltage regulation only; point E with a strategy of peak shaving only. The points in between represent trade-off strategies. This is reflected in the distribution of $|U_{p,60,k}|$ and of $|S_{p,k}^{\mathrm{tot}}|$ in Fig. 6. Also, the design variable S_{nom} is larger in A than in E. Conversely, E_{nom} is larger in E than in A.

The largest amount of reactive power, $Q_{p,k}^{\mathrm{inv}}$, is used for voltage regulation in A, with a peak value of $20.5\,\mathrm{kvar}$ in each phase. The peak shaving objective is counteracted by this reactive power injection, and is even worse than the no-BESS solution.

In point A, there is a peak active power flow $P_{p,k}^{\mathrm{inv}}$ of $-17.7\,\mathrm{kW}$ in phase 2, although the dc-link nominal power $P_{\mathrm{nom}}^{\mathrm{dc}}$ is only $3.36\,\mathrm{kW}$. This means that, when this peak occurs, the power drawn from the grid in phase 2 is redistributed, and injected in the other phases of the grid. This mechanism of inter-phase exchange of active power allows an inverter to provide active power, without using batteries.

The second curve in Fig. 5, from F to I, depicts the inverter-only solution. When compared with the other curve, E has a better peak shaving objective than I, due to the additional active power provided by the batteries. Both attain the same optimal voltage regulation index in A and F. However, in F, the corresponding peak shaving objective is worse. Moving from F to I on the curve, the inverter-only peak-shaving objective reaches a technical limit, because from a certain point on, the grid power is balanced and a source of active power is required for further peak shaving (see $P_{p,k}^{\mathrm{inv}}$ for E and I). Because of this technical limit, there is no use to invest more in S_{nom}, which is the only free design variable. Therefore, the maximum allowed cost of €5000 per year is not reached for the inverter-only solution, except in point F (see K_{tot} in Fig. 6).

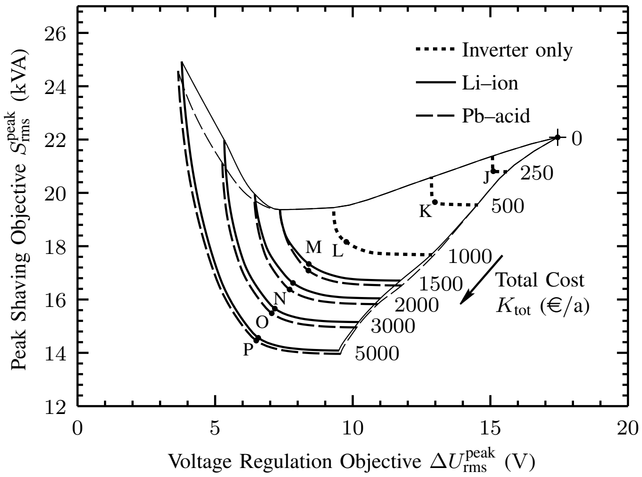

Fig. 7. Pareto-optimal isocost trade-off curves between the objectives of peak shaving and voltage regulation, computed for two battery technologies, for multiple annual costs K_{tot}. The BESS is located at node 17.

C. Battery Technology Comparison

In Fig. 7, isocost trade-off curves for two battery technologies are depicted for multiple costs K_{tot}. The points J to P correspond to knee-point trade-off strategies for increasing cost, and their decision variables are shown in Fig. 8. For a K_{tot} from €0 to €1000 per year the algorithm converges to a BESS with zero battery capacity E_{nom}, and consequently, the optimal solution to provide grid services is an inverter without batteries (points J to L).

Starting from a cost of €1500 per year, the algorithm converges to solutions with non-zero battery capacity (M to P). Therefore, these solutions dominate inverter-only solutions with the same cost.

Fig. 7 shows that the Pb–acid technology dominates Li–ion, but the difference between both technologies is small, relative to the no-BESS solution (point 0). As a result, the technology selection can in practice be based on secondary design requirements such as volume, weight and calendar life $\tau^{\text{bat}}_{\text{E}}$. Fig. 8 reveals that the calendar life of Li–ion batteries is limited by the shelf-life in M and N, but limited by the cycle life in O and P. The calendar life of Pb–acid is always limited by the cycle life. Although Pb–acid is cycled less frequently, the calendar life is lower than for Li–ion.

Because of the small difference in objective values between technologies, and consequently the small variations in $P^{\text{inv}}_{p,k}$ and $Q^{\text{inv}}_{p,k}$, the inverter nominal power values S_{nom} are similar as well. However, the nominal battery capacity E_{nom} and dc-link nominal power $P^{\text{dc}}_{\text{nom}}$ are much higher for Pb–acid than for Li–ion. In point P, E_{nom} is 11.6 kWh and $P^{\text{dc}}_{\text{nom}}$ is 12.0 kW for Li–ion. For Pb–acid, E_{nom} is 19.3 kWh and $P^{\text{dc}}_{\text{nom}}$ is 19.3 kW. Nevertheless, because of the $1/3$ charge power-to-energy ratio for Pb–acid (see Table II), the charge power is constrained to 6.4 kW.

Moving from J to P, S_{nom} increases with K_{tot} and therefore, losses also increase. From J to L, the energy cost, K_{E}, increases because K_{E} is solely determined by inverter losses. From M to P, however, K_{E} reaches a maximum in O for Li–ion and in N for Pb–acid. Because of increasing storage capacity,

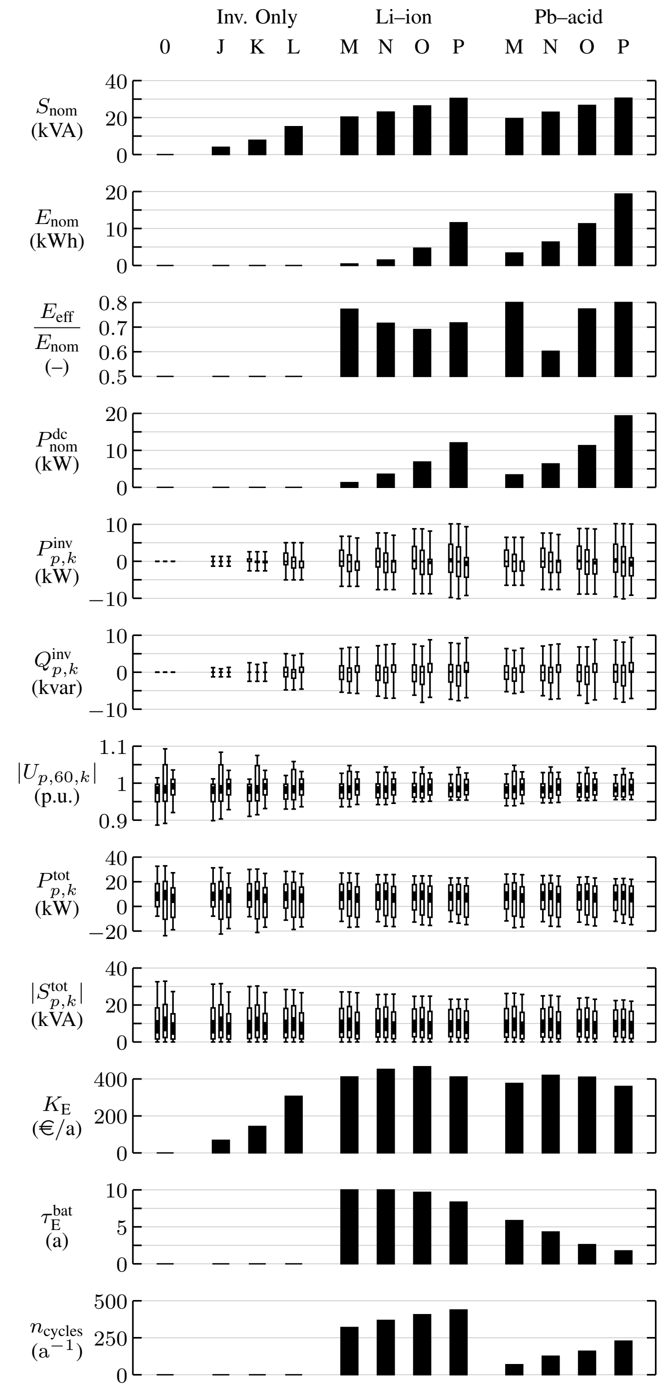

Fig. 8. Decision variables for the solutions J to P depicted in Fig. 7.

there is more flexibility to schedule the battery cycling based on the electricity price, resulting in a reduction of K_{E}.

For both Li–ion and Pb–acid solutions are found where $E_{\text{eff}}/E_{\text{nom}}$ converges to a value lower than 0.8, as seen in the corresponding row of Fig. 8. Table IV presents a sensitivity analysis of K_{tot} in point P, to -10 % and $+10$ % perturbations of the ratio $E_{\text{eff}}/E_{\text{nom}}$, the cycle life parameter n_{80}, and specific battery cost $c^{\text{bat}}_{\text{E}}$, while all other parameters are kept constant. The sensitivity to the design parameter $E_{\text{eff}}/E_{\text{nom}}$ is small, compared to the technology dependent parameters n_{80} and $c^{\text{bat}}_{\text{E}}$.

TABLE IV
SENSITIVITY ANALYSIS IN POINT P

	Li–ion		Pb–acid	
Perturbation	-10 %	$+10$ %	-10 %	$+10$ %
K_{tot} sensitivity to $E_{\text{eff}}/E_{\text{nom}}$	$+0.58$ %	$+0.162$ %	$+0.67$ %	–
K_{tot} sensitivity to n_{80}	$+3.08$ %	-2.52 %	$+6.12$ %	-5.01 %
K_{tot} sensitivity to $c_{\text{E}}^{\text{bat}}$	-5.08 %	$+5.08$ %	-6.47 %	$+6.47$ %

VI. CONCLUSION

By installing a BESS in LV residential distribution feeders with overvoltage problems, voltage deviations can be reduced to facilitate further integration of PV, thereby avoiding automatic disconnection of inverters. The results of this research illustrate trade-offs between three objectives: voltage regulation, the reduction of peak apparent power, and annual cost. The proposed method serves as a tool in the decision-making process to install a BESS. The method determines the cost corresponding to a required technical performance. In a cost-benefit analysis, the value of these technical services should be considered as well [31]. For example, a grid operator can decide to temporarily install a BESS in problematic feeders, in order to postpone grid upgrades in the short term due to work planning issues. When the grid operator compares the cost of grid upgrades, it is possible that the BESS is also a valuable alternative in the long term.

Before the optimization method is applied, the grid conditions should be analyzed and a connection point should be selected, preferably not too close to the distribution transformer (Fig. 4). With the proposed optimization method, inverter size and battery size are determined together with the control variables. It is found that in some cases, solutions without batteries are optimal (Fig. 7). In those cases, the reactive and active power flow is controlled by the inverter only. The active power flow is provided by exchange of power between phases. Solutions with batteries become optimal when a higher technical performance is required (in the presented scenario at a cost of €1500). The difference between the results of Li–ion and Pb–acid is small. Furthermore, the sensitivity of the results to the E_{eff} to E_{nom} ratio is also small. Therefore, the selection of technology and the E_{eff} to E_{nom} ratio can be based on other decision factors: expected battery lifetime, battery volume and weight, initial investment cost, and expertise. Next to Li–ion and Pb–acid batteries, other storage technologies could be considered [32].

In the proposed optimization method, knowledge of all time profiles is assumed. In practice, a short term and long term control method would be required to operate the BESS. The short term control method controls the BESS power flow and performs the battery state of charge estimation [33]. For the implementation of long term control, rule-based or prediction-based methods have been proposed [12], [34]. The long term control strategy can be benchmarked with the optimization result, which gives the best possible solution.

An alternative approach is to install batteries at locations where a PV inverter is already present [8], [12]. However, PV inverters in Belgium are often single-phase, and three-phase inverters are balanced. Such inverters cannot make use of power exchange between phases. A second alternative is to use the batteries of locally parked electric vehicles, which has been widely addressed through the concept of vehicle to grid [26], [35]. In this approach, the battery size is fixed and optimized for the driving application. Furthermore, availability and energy content of the battery are influenced by driving behavior. In order to allow power exchange between phases, a bidirectional charger with unbalanced three-phase control would be needed.

In this research, the common battery manufacturer definition for battery end of life was used: batteries are replaced when the usable capacity falls below 80 % of the nominal battery capacity. In [22], it is questioned whether this definition is justified, because such a replaced battery is still usable with a reduced effective energy capacity E_{eff}. Therefore, the estimated calendar life in the results is underestimated. If the batteries were to be replaced at 80 % of the nominal battery capacity, there may still be a second life value. In this case, the depreciation cost is overestimated.

APPENDIX
REGULAR POLYGON APPROXIMATION OF A CIRCULAR CONSTRAINT

The constraint needed to limit two variables x and y to a circular region with radius r is quadratic and of the form

$$x^2 + y^2 \leq r^2. \tag{26}$$

The circular region can be approximated with a set of n linear constraints representing an n-sided regular polygon:

$$Re\left((x + \text{j}y)\,\text{e}^{\text{j}\frac{2\pi k}{n}}\,\text{e}^{\text{j}\frac{\pi}{n}}\right) \leq ar, \quad k = 1, \ldots, n \tag{27}$$

where a is a scaling parameter chosen equal to 1 for a circumscribed polygon and equal to $\cos\frac{\pi}{n}$ for an inscribed polygon.

REFERENCES

[1] B. P. Roberts and C. Sandberg, "The role of energy storage in development of smart grids," *Proc. IEEE*, vol. 99, no. 6, pp. 1139–1144, Jun. 2011.

[2] J. Eyer, "Electric utility transmission and distribution upgrade deferral benefits from modular electricity storage," Sandia National Laboratories, Tech. Rep. SAND2009-4070, Jun. 2009.

[3] E. Peeters, C. Develder, J. Das, J. Driesen, and R. Belmans, "LINEAR: towards a breakthrough of smart grids in flanders," in *Proc. 2nd Int. Conf. Innovation for Sustainable Production*, vol. 3, Bruges, Belgium, 2010, pp. 3–6.

[4] M. Thomson and D. Infield, "Impact of widespread photovoltaics generation on distribution systems," *IET Renew. Power Gener.*, vol. 1, no. 1, p. 33, 2007.

[5] Y. Ueda, K. Kurokawa, T. Tanabe, K. Kitamura, and H. Sugihara, "Analysis results of output power loss due to the grid voltage rise in grid-connected photovoltaic power generation systems," *IEEE Trans. Ind. Electron.*, vol. 55, no. 7, pp. 2744–2751, Jul. 2008.

[6] M. Braun, G. Arnold, and H. Laukamp, "Plugging into the zeitgeist," *IEEE Power Energy Mag.*, vol. 7, no. 3, pp. 63–76, May 2009.

[7] R. D'hulst and E. Peeters, "Distributed voltage control strategies in a LV distribution network," in *Proc. Int. Conf. Renewable Energies and Power Quality*, Granada, Spain, 2010, paper 389.

[8] K. Büdenbender, M. Braun, T. Stetz, and P. Strauss, "Multifunctional PV systems offering additional functionalities and improving grid integration," *Int. J. Distributed Energy Resources*, vol. 7, no. 2, pp. 109–128, 2011.

[9] M. Braun, T. Stetz, R. Bründlinger, C. Mayr, K. Ogimoto, H. Hatta, H. Kobayashi, B. Kroposki, B. Mather, M. Coddington, K. Lynn, G. Graditi, A. Woyte, and I. MacGill, "Is the distribution grid ready to accept large-scale photovoltaic deployment? state of the art, progress, and future prospects," *Prog. Photovolt: Res. Appl.*, 2011.

[10] *Specifieke Technische Voorschriften Voor Decentrale Productie-Installaties die in Parallel Werken met het Distributienet*, Synergrid regulation C10/11, Rev. 12, May 2009.

[11] *Automatic disconnection device between a generator and the public low-voltage grid*, DIN VDE Std. 0126-1-1, Feb. 2006.

[12] Y. Riffonneau, S. Bacha, F. Barruel, and S. Ploix, "Optimal power flow management for grid connected PV systems with batteries," *IEEE Trans. Sustainable Energy*, vol. 2, no. 3, pp. 309–320, Jul. 2011.

[13] R. Cremers and G. Bloemhof, "Storage optimization in distribution systems," in *Proc. 21st Int. Conf. Exhibition Electricity Distribution (CIRED)*, Frankfurt, Germany, 2011, paper 0180.

[14] F. Geth, J. Tant, E. Haesen, J. Driesen, and R. Belmans, "Integration of energy storage in distribution grids," in *Proc. IEEE Power and Energy Soc. General Meeting*, Minneapolis, MN, Jul. 2010.

[15] F. Geth, J. Tant, T. De Rybel, P. Tant, D. Six, and J. Driesen, "Techno-economical and life expectancy modeling of battery energy storage systems," in *Proc. 21st Int. Conf. Exhibition Electricity Distribution (CIRED)*, Frankfurt, Germany, 2011, paper 1106.

[16] *Kabels Voor Ondergrondse Aanleg, met Synthetische Isolatie en Versterkte Mantel (Type 1kV)*, NBN Std. C 33-322, 1975.

[17] C. Cheng and D. Shirmohammadi, "A three-phase power flow method for real-time distribution system analysis," *IEEE Trans. Power Syst.*, vol. 10, no. 2, pp. 671–679, 1995.

[18] *Voltage Characteristics of Electricity Supplied by Public Electricity Networks*, CENELEC Std. EN 50 160, Jul. 2010.

[19] B. Dupont, C. De Jonghe, K. Kessels, and R. Belmans, "Short-term consumer benefits of dynamic pricing," in *Proc. 8th Int. Conf. European Energy Market*, Zagreb, Croatia, May 2011, pp. 216–221.

[20] "Market monitor 2010," Flemish Regulator of the Electricity and Gas market (VREG), Tech. Rep. REP-2010-1, Oct. 2010.

[21] M. Aredes, J. Hafner, and K. Heumann, "Three-phase four-wire shunt active filter control strategies," *IEEE Trans. Power Electron.*, vol. 12, no. 2, pp. 311–318, Mar. 1997.

[22] J. D. Dogger, B. Roossien, and F. D. J. Nieuwenhout, "Characterization of Li-ion batteries for intelligent management of distributed grid-connected storage," *IEEE Trans. Energy Convers.*, vol. 26, no. 1, pp. 256–263, Mar. 2011.

[23] "WP1.3 parameter manual," Grid For Vehicles, Proj. Rep., Dec. 2010. [Online]. Available: http://www.g4v.eu

[24] W. Kempton and J. Tomić, "Vehicle-to-grid power fundamentals: Calculating capacity and net revenue," *J. Power Sources*, vol. 144, no. 1, pp. 268–279, Jun. 2005.

[25] K.-H. Ahlert, "Economics of distributed storage systems," Ph.D. dissertation, Karlsruher Institut Für Technologie, 2010.

[26] A. G. Boulanger, A. C. Chu, S. Maxx, and D. L. Waltz, "Vehicle electrification: Status and issues," *Proc. IEEE*, vol. 99, no. 6, pp. 1116–1138, Jun. 2011.

[27] J. Cao and A. Emadi, "Batteries need electronics," *IEEE Ind. Electron. Mag.*, vol. 5, no. 1, pp. 27–35, Mar. 2011.

[28] J. Siemer, "Inverter price index," *Photon Int.*, pp. 82–84, Oct. 2011.

[29] A. Ristow, M. Begovic, A. Pregelj, and A. Rohatgi, "Development of a methodology for improving photovoltaic inverter reliability," *IEEE Trans. Ind. Electron.*, vol. 55, no. 7, pp. 2581–2592, Jul. 2008.

[30] J. Löfberg, "YALMIP: a toolbox for modeling and optimization in MATLAB," in *Proc. 2004 IEEE Int. Symp. Computer Aided Control Systems Design*, Taipei, Taiwan, pp. 284–289.

[31] "Electric energy storage technology options: A white paper primer on applications, costs, and benefits," EPRI, Palo Alto, CA, Tech. Rep. 1020676, Dec. 2010.

[32] S. Vazquez, S. M. Lukic, E. Galvan, L. G. Franquelo, and J. M. Carrasco, "Energy storage systems for transport and grid applications," *IEEE Trans. Ind. Electron.*, vol. 57, no. 12, pp. 3881–3895, Dec. 2010.

[33] H. Qian, J. Zhang, J. Lai, and W. Yu, "A high-efficiency grid-tie battery energy storage system," *IEEE Trans. Power Electron.*, vol. 26, no. 3, pp. 886–896, Mar. 2011.

[34] S. Teleke and M. Baran, "Rule-based control of battery energy storage for dispatching intermittent renewable sources," *IEEE Trans. Sustainable Energy*, vol. 1, no. 3, pp. 117–124, Oct. 2010.

[35] W. Kempton and S. E. Letendre, "Electric vehicles as a new power source for electric utilities," *Transpn Res.-D*, vol. 2, no. 3, pp. 157–175, Sep. 1997.

Jeroen Tant (S'08) received the M.Sc. degree in Electrical Engineering from the University College Howest, Kortrijk, Belgium, in 2007 and the M.Sc. degree in Mathematical Engineering from the KU Leuven, Leuven, Belgium, in 2009. He is currently working towards the Ph.D. degree at the KU Leuven. He holds a Ph.D. fellowship from the Research Foundation Flanders (FWO). His research topics include the simulation, modeling, and optimization of power electronic systems and power distribution grids.

Frederik Geth (S'10) received the M.Sc. degree in Electrical Engineering from the KU Leuven, Leuven, Belgium, in 2009. Since 2009, he is working towards the Ph.D. degree, as a research assistant with the division ESAT-ELECTA. His research interests include electrical storage in distribution grids, batteries for (hybrid) electric vehicles and modeling of the impact of the charging of plug-in electric vehicles in the distribution grid.

Daan Six received the M.Sc. degree in commercial engineering from the University of Antwerp, Antwerp, Belgium, in 2004. He is currently with the Energy Technology department of the Flemish Institute for Technological Research (VITO), Belgium. After conducting research in the field of energy markets and business modeling for smart grids, he became project manager in 2009. He is currently supervising the research activities in the field of electric energy storage and advanced techno-economic business case assessments for innovative energy technologies.

Peter Tant received the M.Sc. degree from the University College Howest, Kortrijk, Belgium, in 2003 and the M.Sc. and Ph.D. degree from the KU Leuven, Leuven, Belgium in 2005 and 2010 respectively, in electrical engineering. He is a researcher at the Electrical Energy research Group, ELECTA, of the department of electrical engineering of KU Leuven since 2005. His research interests are in the field of power electronics, measurement techniques and smart grid technologies.

Johan Driesen (S'93 - M'97 - SM'12) received the M.Sc. and Ph.D. degrees in Electrical Engineering from the KU Leuven, Leuven, Belgium, in 1996 and 2000, respectively. Currently, he is a Professor with the KU Leuven and teaches power electronics and electric drives. In 2000, he was with the Imperial College of Science, Technology and Medicine, London, U.K. In 2002, he was with the University of California, Berkeley. Currently, he conducts research on distributed generation, power electronics, and its applications.